

Effect of pre-corrosion on Electrochemical Corrosion and Fatigue Behavior of S135 High-Strength Drill Pipe Steel in Marine Environment

Sheji Luo^{1,*}, Ming Liu^{2,3,*}, Ninhua Wen⁴, Yi Shen¹, Yanming Liu¹, Xiuzhou Lin⁵

¹ School of Materials Science and Engineering, Xi'an Shiyou University, Xi'an 710065, PR China

² State Key Laboratory for Mechanical Structure Strength and Vibration Xi'an Jiaotong University, Xi'an 710049, PR China

³ MOE Key Laboratory for Multifunctional Materials and Structures, Xi'an Jiaotong University, Xi'an 710049, PR China

⁴ Anke Engineering Technology Research Institute (Beijing) Co, Ltd., Beijing, 100083, PR China

⁵ Material Corrosion and Protection Key Laboratory of Sichuan province, Sichuan University of Science and Engineering, Zigong 643000, PR China

*E-mail: sjluo@xsyu.edu.cn (Sheji Luo), liuming0313@xjtu.edu.cn (Ming Liu)

Received: 5 November 2018 / Accepted: 17 December 2018 / Published: 7 February 2019

The pre-corrosion on electrochemical corrosion and fatigue behaviors of S135 drill pipe steel were tested in simulated marine environment. The results shows that no passivation can be observed. With the extension of the immersion time, open circuit potential of the steel moves to the negative direction, the charge transfer resistance decreases, and both the corrosion current density and the corrosion rate increase. With the increasing of the pre-corrosion time, more larger and deeper corrosion pits are formed, the corrosion products are mainly constituted of Fe₂O₃, FeO(OH) and Fe₃O₄, which are porous and not adhering tightly to the steel substrate. With the increasing of the immersion time, the fatigue life of S135 steel is significantly reduced, and the fatigue cracks initiate at or near the corrosion pits and multiple crack sources could be observed. Cleavage steps and fatigue striations are the main features in the crack propagation zone, the fatigue striations become more obvious and the spacing of striations become smaller with the decreasing of stress amplitudes.

Keywords: S135 drill pipe steel; marine environment; fatigue lives; corrosion pit

1. INTRODUCTION

With the gradually exhausting of shallow oil and gas resources, the speed of oil exploitation has slowed down. Therefore, ultra-deep and other high-difficulty wells have become the main targets of the

world's oil and gas fields [1–3]. Due to the limitation of offshore oil and gas development environment, corrosion occurs throughout the whole mining process [4–7]. From mining, transportation and other processes are accompanied by the damage of seawater corrosion. All kinds of special tubing and mechanical equipment used in drilling process are in the environment prone to electrochemical corrosion, and most of the materials in the drilling process are under alternating load [8,9]. Mechanical loading will aggravate corrosion and cause fatigue failure. Fatigue of drill pipe is a common accident in drilling process, which seriously restricts the drilling speed and increases the drilling cost.

Researchers [10–13] have studied the microstructure, heat treatment process and fatigue fracture of drill pipe steel, which have obtained some theoretical and practical experiences. However, the failure caused by pre-corrosion defects of drill pipe steel has been neglected. The existence of corrosion defects shorten the crack growth period and greatly increase the crack growth rate. Generally, fatigue cracks are initiated at the corrosion pits, and there are obvious corrosion marks around the crack source. Corrosion pits of drill pipes may be formed during using or storage process [14,15]. The main corrosive media is drilling fluid. When the drilling pipe is stored, the residual drilling fluid and atmospheric environment will corrode the drill pipe, which is sometimes even more serious than the corrosion in drilling fluid [16,17]. If there is corrosion pit before drilling, the fatigue crack initiation period will be greatly shortened. At present, the research on fatigue life and fracture mechanisms of drill pipe after pre-corrosion are rarely reported. In order to make drill pipe safer and more effective in practical work, it is essential to study the influence of pre-corrosion on the fatigue life and fracture mechanism of drill pipe steel.

In our previous work, the biaxial fatigue behavior under combined axial and torsional loading for S135 drill pipe steel in air was studied [18]. We find that the fatigue life regulation of S135 drill pipe steel can be represented well by the fatigue life equation, and the fracture surfaces are mainly divided into three regions. Fatigue cracks mainly initiate at the specimen surface and the fracture surfaces are characteristic of river patterns at crack initiation region. In order to supplement the previous work, the open circuit potential (OCP), potentiodynamic polarization and electrochemical impedance spectroscopy are employed to obtain the electrochemical characteristics of steel after various immersion time, the fatigue life and fracture morphology of the samples after different pre-corrosion time are observed. The fracture mechanisms of pre-corrosion on drill pipe steel are summarized.

2. EXPERIMENTAL

2.1. Materials and solution

In this work, S135 high-strength carbon drill pipe steel was used for experiments. Its chemical constituents (mass fraction /%) are 0.20 C, 0.24 Si, 0.54 Mn, 0.007 P, 0.0035 S, 0.403 Ni, 0.861 Cr, 0.858 Mo, 0.007 Ti, 0.06 Cu, remaining Fe. Samples for electrochemical and immersion tests had dimensions of 10 mm×10 mm×5 mm and 25 mm×20 mm×3 mm respectively. For electrochemical test sample, the exposed measurement area was 10 mm×10 mm, which was retained by epoxy resin. Prior to the experiment, the samples were polished with silicon carbide water polishing papers down to 2000#.

Then, the samples were ultrasonically cleaned in acetone and rinsed in distilled water. The round bar fatigue specimen is intercepted on the drill pipe. The shape and size of the specimen are shown in Fig. 1, and the length of the specimen is in the longitudinal direction of the drill pipe.

The 3.5 wt.% NaCl solution was chosen to simulate the marine environment. The NaCl was dissolved in deionized water with a pH of approximately 6.8–7.0. Prior to the experiment, all the specimens were pre-corrosion in 3.5 wt.% NaCl solution for 10, 30 and 60 days to simulate the actual working conditions.

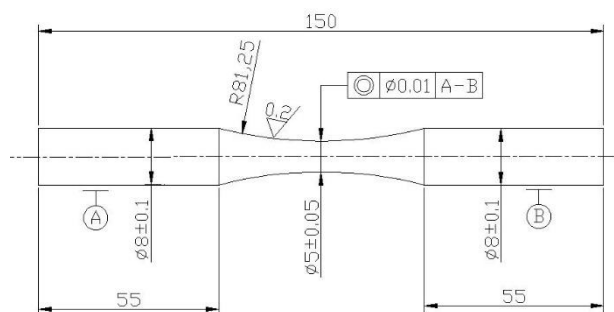


Figure 1. Schematic illustrations of the fatigue specimen (all units are in mm).

2.2. Electrochemical measurements

Electrochemical tests were performed using the PARSTAT 2273 electrochemical workstation. A three-electrode system was applied, with S135 steel serving as the working electrode, the saturated calomel electrode (SCE) as the reference electrode, and a platinum gauge as the counter electrode. Potentiodynamic polarization were measured from -950 mV (Vs. SCE) to the potential where the anodic current density attained $100 \mu\text{A}\cdot\text{cm}^{-2}$, with a scanning rate of $0.2 \text{ mV}\cdot\text{s}^{-1}$. EIS tests were performed at OCP with a scanning range of $100 \text{ kHz} - 10 \text{ mHz}$ at the amplitude of 10 mV , and the results were analyzed with ZsimpWin Software. All tests were conducted at ambient temperature (25 ± 1 °C). Each test was performed thrice to ensure the repetitiveness of the results.

2.3. Immersion test

Scanning electron microscopy (SEM, JSM-6390A) was used to observe the macroscopic corrosion morphology. The corrosion rate was calculated by weight loss method. The corrosion products were analyzed by X-ray diffraction using Cu $K\alpha$ radiation with $\lambda = 0.154 \text{ nm}$ operated at 40 kV and 40 mA with a scanning range of $10^\circ - 90^\circ$. The corrosion products were mechanically scraped and ground into powders less than $10 \mu\text{m}$ to obtain fine grain size without any preferred orientation. Before the X-ray diffraction (XRD) test, the glass plate was filled with powdered corrosion products, and acetone was dripped into the plate for fixation.

2.4. Fatigue test

To investigate the fatigue behavior and mechanisms of S135 steel after pre-corrosion, fatigue tests were performed on the PLD-100 microcomputer controlled electro-hydraulic servo fatigue test machine with the triangular wave. The experimental frequency is 5Hz, and the stress ratio R is 0.1. In the fatigue test, the normal stress σ applied to the specimen is calculated by the following equation:

$$\sigma = \frac{P}{S} \quad (1)$$

Where P is applied load; S is the cross-section area of the specimen.

After the experiment, fracture morphologies were observed by SEM (JSM-6390A). All tests were conducted at the ambient temperature (approximately 25 °C).

3. RESULTS AND DISCUSSION

3.1. Electrochemical corrosion behaviors

3.1.1 Open circuit potential

Figure 2 shows OCP of S135 steel after pre-corrosion in 3.5 wt.% NaCl solution for 10, 30 and 60 days. It can be seen that the OCP of S135 steel shifts negatively with the increasing of the corrosion time. The OCP tends to be stable after 2 h immersion, and reaches a stable value at -639 mV after 5 h immersion for the no pre-corrosion sample. The OCP of pre-corrosion samples are relative stable, and the values of OCP are -663, -794 and -823 mV for S135 steel after pre-corrosion for 10, 30 and 60 days respectively. The electrochemical corrosion thermodynamic stability of S135 steel can be preliminarily judged by OCP, the corrosion tendency of S135 steel increases with the increasing pre-corrosion time [19].

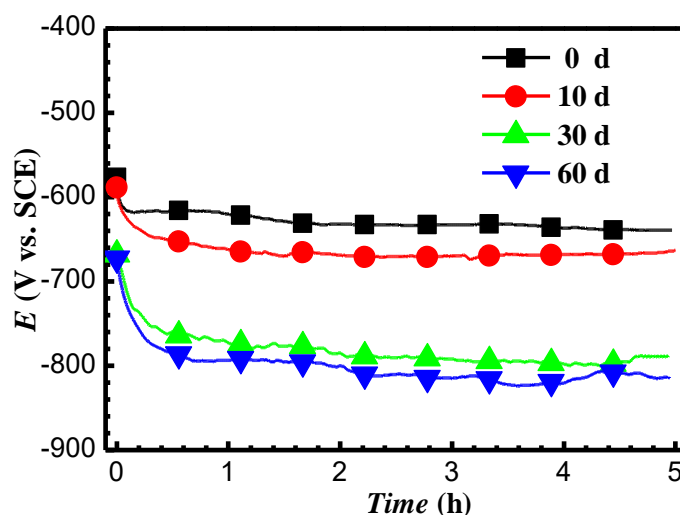


Figure 2. OCP of S135 steel after immersion in 3.5 wt.% NaCl solution for different times (0 day, 10 days, 30 days and 60 days).

3.1.2 EIS

The EIS diagrams of S135 steel after pre-corrosion in 3.5 wt.% NaCl solution for 10, 30 and 60 days are displayed in Fig. 3. It can be seen in Fig. 3(a) that Nyquist plots of steel are incomplete semicircle. The Bode diagrams with a wide phase angle in Fig. 3(b) indicate that there are at least two time constants [20–22]. The low frequency capacitance and impedance arcs are related to the double layer capacitance and charge transfer resistance. The radius of the impedance arc decreases gradually with the pre-corrosion time, which indicates that the corrosion degree of the steel increases with the prolonging of pre-corrosion time.

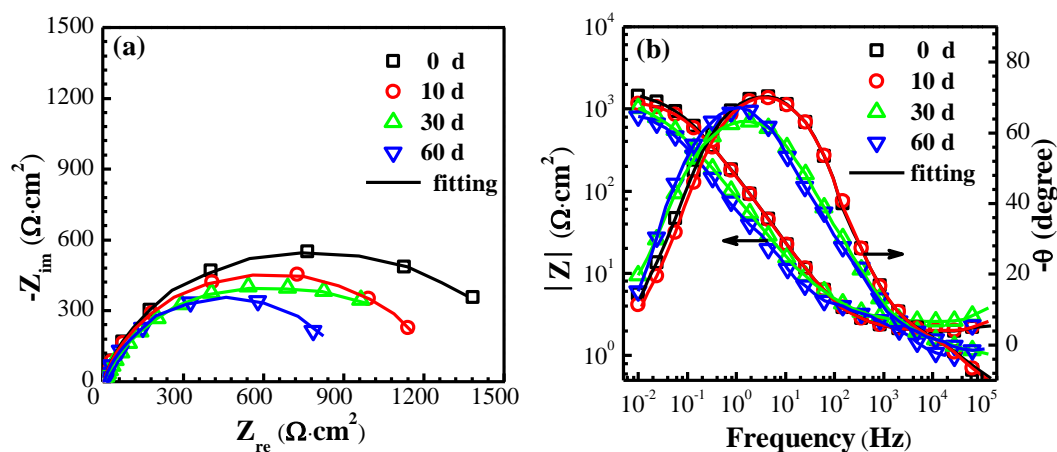


Figure 3. Nyquist (a) and Bode (b) diagrams of S135 steel pre-corrosion in 3.5 wt.% NaCl solution for different times (0 day, 10 days, 30 days and 60 days).

The two time constants equivalent circuit in Fig. 4 was used to fit the EIS data [20–22], where R_s is the solution resistance, R_{ct} is the charge transfer resistance, Q_{dl} is the double layer capacitance of reaction interface, Q_f is the capacitance of corrosion product film, R_f is the resistance of the corrosion product film. The fitting line are also plotted in Fig. 3, and the fitting results are very consistent with the experimental results indicating the feasible of the equivalent circuit.

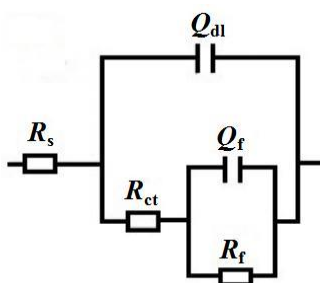


Figure 4. Equivalent circuit of S135 steel after pre-corrosion in 3.5 wt.% NaCl solution for different times (0 day, 10 days, 30 days and 60 days).

The fitting results of the EIS parameters of S135 steel after pre-corrosion in 3.5 wt.% NaCl solution for different times are listed in Table 1. It can be seen that R_{ct} changes little ranging from 2–3

$\Omega \cdot \text{cm}^2$; R_{ct} is between 1019–1564 $\Omega \cdot \text{cm}^2$, and R_f is at 18–36 $\Omega \cdot \text{cm}^2$. By increasing the pre-corrosion time, Q_{dl} of the steel increases, which indicates that the surface of electrode become inhomogeneous; R_{ct} decreases obviously and R_f increases slightly suggesting that no protective corrosion product is formed after long-term immersion. The polarization resistance R_p ($R_p = R_{ct} + R_f$) is often used to evaluate the corrosion resistance of materials [23–25], the greater R_p values, the higher corrosion resistance of the material. As shown in Table 1, the R_p values of the steel decreases with the pre-corrosion time revealing that the corrosion resistance of S135 steel decreases with the pre-corrosion time, which is consistent with the previous OCP testing results.

Table 1. EIS parameters of S135 steel after pre-corrosion in 3.5wt.% NaCl solution for different times (0 day, 10 days, 30 days and 60 days).

Pre-corrosion, Days	R_s , $\Omega \cdot \text{cm}^2$	R_{ct} , $\Omega \cdot \text{cm}^2$	Q_{dl} , $Y_0 (\times 10^{-6})$ $\Omega^{-1} \cdot \text{cm}^{-2} \cdot \text{s}^n$	n	R_f , $\Omega \cdot \text{cm}^2$	Q_f , $Y_0 (\times 10^{-6})$ $\Omega^{-1} \cdot \text{cm}^{-2} \cdot \text{s}^n$	n
0	2.09	1564	230	0.98	18	126	0.73
10	2.11	1389	242	0.81	21	350	0.64
30	2.09	1273	293	0.74	24	226	0.62
60	3.39	1019	370	0.95	36	369	0.65

3.1.3 Polarization curve

The polarization curves of S135 steel after pre-corrosion for 10, 30 and 60 days in 3.5 wt.% NaCl solution are presented in Fig. 5. It is clear that all curves show the active corrosion without passivation. Additionally, the self-corrosion potential (E_{corr}) of the steel has the same changing trend as the OCP, which becomes more and more negative with the prolongation of the pre-corrosion process. E_{corr} is the corresponding potential when the current density is zero, where the number of electrons in the cathodic is equal to that in the anodic reaction [31]. Although the variation trend of OCP is consistent with that of E_{corr} , OCP is measured without external current. With the prolongation of the pre-corrosion time, the polarization curve moves to the bottom right, which indicates that the corrosion rate increases with the increasing of i_{corr} .

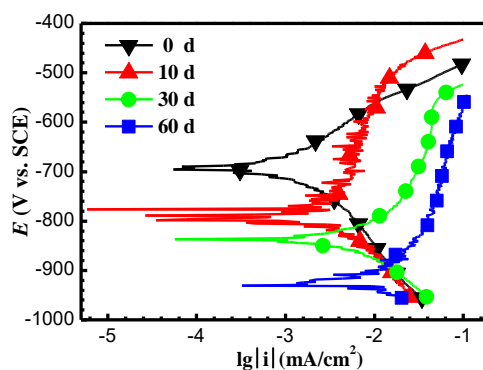


Figure 5. Polarization curves of S135 steel pre-corrosion in 3.5 wt.% NaCl solution for different times (0 day, 10 days, 30 days and 60 days).

According to the relationship between the current density i and the polarization potential E of the Butler–Volmer equation [19].

$$i = i_{\text{corr}} \left[\exp(2.303\Delta E)/b_a - \exp(-2.303\Delta E)/b_c \right] \quad (2)$$

$$\Delta E = E - E_{\text{corr}} \quad (3)$$

Where i_{corr} is the corrosion current density, b_a is the anode Tafel constant, and b_c is the cathode Tafel constant. b_a , b_c and i_{corr} can be calculated by a iterative fitting program, and the polarization resistance R_p and corrosion rate v are calculated by Eqs. (4) and (5) [19].

$$R_p = \frac{b_a b_c}{2.303(b_a + b_c)i_{\text{corr}}} \quad (4)$$

$$v = 0.327 \frac{M i_{\text{corr}}}{n\rho} \quad (5)$$

Where the atomic weight M is 56 for the steel, the density of metal ρ is 7.87 g/cm³, the electrode reaction n is 2, and the unit of i_{corr} is mA/cm².

The electrochemical parameters obtained from fitting the polarization curve data are shown in Table 2. As the pre-corrosion time increases from 10 to 60 days, the i_{corr} increases from 1.664 to 8.794 $\mu\text{A}/\text{cm}^2$, indicating that the steel samples are seriously corroded by the increasing pre-corrosion time. The absolute values of b_c at 0 and 10 days are greater than that of b_a , indicating that the cathode is the control step of the whole electrochemical reaction. However, the b_c values are less than the b_a values at 30 and 60 days, suggesting that the control step is the anode.

Table 2. The electrochemical parameters of S135 steel after pre-corrosion for different times (0 day, 10 days, 30 days and 60 days) in 3.5 wt.% NaCl solution obtained from the polarization curves.

Pre-corrosion, days	E_{corr} , mV	b_a , mV/dec	b_c , mV/dec	i_{corr} , $\mu\text{A}/\text{cm}^2$	v , $\mu\text{m}/\text{a}$
0	-696	114	-152	1.376	15.70
10	-787	89	-138	1.664	19.12
30	-837	191	-137	6.612	75.96
60	-931	135	-81	8.794	93.59

3.2. Immersion test

In the immersion test, the corrosion products are easily to fall off from the surface of the sample, and the remaining corrosion products on the steel surface are also very loose and easy to fall off. The corrosion morphology of the samples after corrosion for 10, 30 and 60 days are shown in the Fig. 6. The corrosion rate is calculated by the weight loss method, and the results are presented in Fig. 7. It can be seen that the corrosion rate of S135 steel is 6.92, 8.85 and 13.4 $\mu\text{m}/\text{a}$ after 10, 30 and 60 days immersion in 3.5 wt.% NaCl solution, respectively. With the increasing of the corrosion time, the corrosion rate of S135 steel increases. According to NACE RP 07799 standard, the corrosion rate of S135 steel is in the low range [26]. The corrosion products will fall off from the sample surface due to their loose feature when their thickness increases to a certain level. Moreover, Cl^- in solution can easily react with the

sample through the porous corrosion products resulting in no hindrance of corrosion rate.

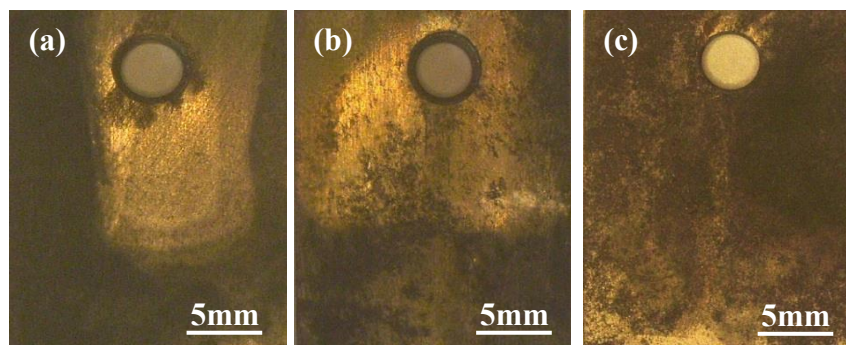


Figure 6. Macroscopic morphology of specimens after corrosion in 3.5 wt.% NaCl solution for different times: (a) 10 days, (b) 30 days and (c) 60 days.

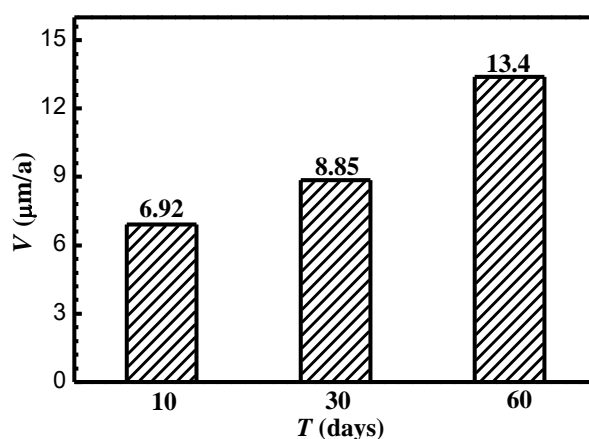


Figure 7. The weight loss corrosion rate of S135 steel after corrosion in 3.5 wt.% NaCl solution for different times (10 days, 30 days and 60 days).

The SEM microscopic morphologies of S135 steel after corrosion for 10, 30 and 60 days in 3.5 wt.% NaCl solution are shown in Fig. 8. The corrosion products have poor bonding ability and are mainly cracked. The corrosion products are loose when the corrosion time is 10 days. There are less corrosion products adhered to the steel surface when the corrosion time is 30 days. The corrosion products are accumulated and begin to fall off when the corrosion time is 60 days. Compared with the corrosion products of 30 days, it is obvious that the corrosion products of 60 days are not complete blocks and the cracks are deeper and larger.

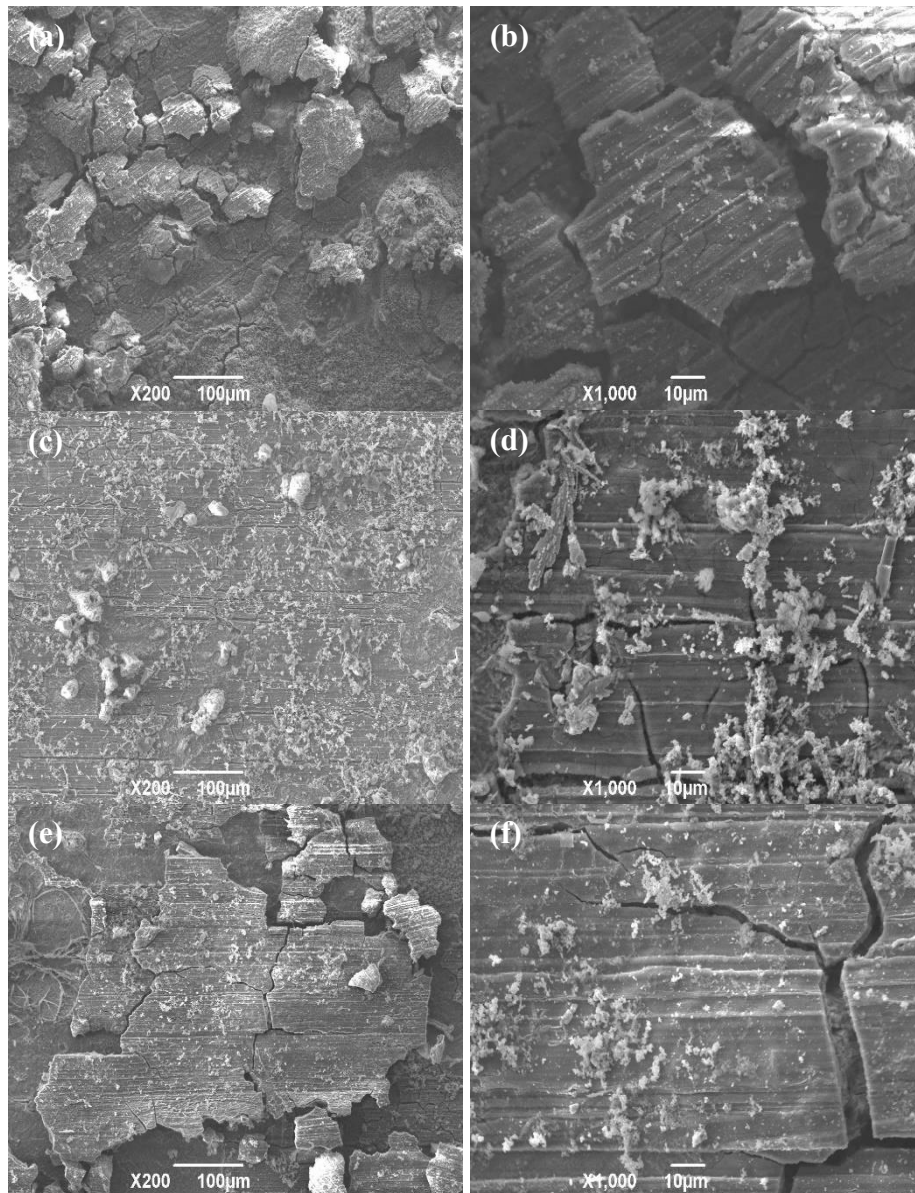
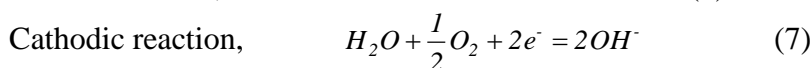
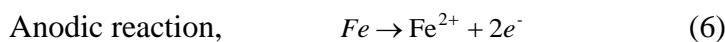
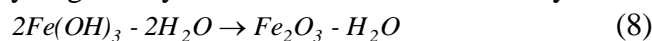


Figure 8. Microscopic morphologies of S135 steel after corrosion in 3.5 wt.% NaCl solution for different times: (a) and (b) 10 days; (c) and (d) 30 days ; (e) and (f) 60 days.

The XRD patterns of the steel corrosion products is presented in Fig. 9. Obviously, the main components of the corrosion products are Fe_2O_3 , $FeO(OH)$ and Fe_3O_4 . The corrosion mechanism of S135 steel in 3.5 wt.% NaCl solution can be deduced as the follows [27,28].



Due to the very unstability, Fe^{2+} are easy to lose an electron and continue to be oxidized to be a higher-valence stable compound $Fe(OH)_3$, and then deposit with a stable compound, but some of the precipitates are easy to get dehydrated to form rust or ferric hydroxide[29,30]:





The black Fe_3O_4 can be formed by $\text{FeO}(\text{OH})$ and further adhered to the steel surface, and the contacting between corrosion solution and material matrix are prevented. During the immersion test, the corrosion products such as the yellow $\text{FeO}(\text{OH})$ and the brown-red Fe_2O_3 can be clearly observed on the surface of the sample, and a large amount of yellow products are precipitated at the bottom of the beaker.

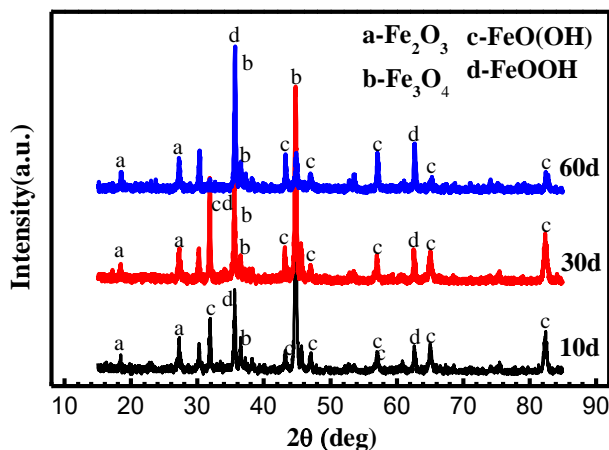


Figure 9. XRD analysis of S135 steel corrosion products after corrosion in 3.5 wt.% NaCl solution for different times (10 days, 30 days and 60 days).

After removing the corrosion products, the surface morphologies of S135 steel after pre-corrosion for different times are shown in Fig. 10. It can be seen that the depth of corrosion pits increases with the increasing pre-corrosion time. The diameter of the corrosion pits is approximately 13, 22 and 25 μm after immersion for 10, 30 and 60 days, respectively. Corrosion pits are caused by the active dissolution of the metal surface inside the pits, the pits outside areas covering corrosion products show low activity, and the large potential difference between these two areas promote the development of the pitting corrosion process [31–33]. The corrosion products around the pits will fall off when they are accumulated to a certain extent, and a new active surface will appear. Similarly, there is a potential difference between the new surface and the surrounding interface, and a corrosion pit will be formed. The small corrosion pits will connect together with the prolonging immersion time leading to the aggravated corrosion process, therefore, the corrosion pits after immersion for 60 days become larger and deeper.

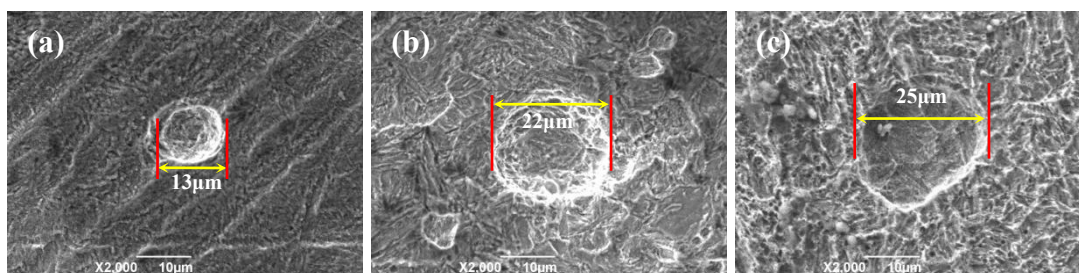


Figure 10. Surface morphologies of S135 steel after removing the corrosion products with pre-corrosion for different days: (a) 10 days, (b) 30 days and (c) 60 days.

3.3. Fatigue behavior

3.3.1. Fatigue life and $S-N$ curve

The fatigue test results and $S-N$ curves of S135 steel under different stress amplitudes after pre-corrosion for 10, 30 and 60 days are shown in Fig. 11. The fatigue life is 2593 and 7.23×10^6 cycles when the σ_{\max} is 1044.5 and 611.4 MPa respectively for the specimens after pre-corrosion for 10 days; the fatigue life is 1932 and 5.66×10^6 cycles when the σ_{\max} is 1044.5 and 611.4 MPa respectively for the specimens after pre-corrosion for 30 days; the fatigue life is 952 and 5.88×10^4 cycles when the σ_{\max} is 1044.5 and 611.4 MPa respectively for the specimens after pre-corrosion for 60 days. Obviously, the fatigue life of S135 steel increases with the decreasing of the stress amplitudes, and the fatigue life decreases with the increasing of the pre-corrosion time. The longer the interval is, the more corrosion pits are formed on the surface of the sample, and the deeper the depth of corrosion pits is. In addition, the cycle of the crack initiation is shortened, the crack initiation is accelerated, and the failure of the drill pipe is accelerated. The result shows that the longer the pre-corrosion time is, the more and deeper corrosion pits will be formed. Meanwhile, the crack initiation period will be shortened, and the failure process will be accelerated.

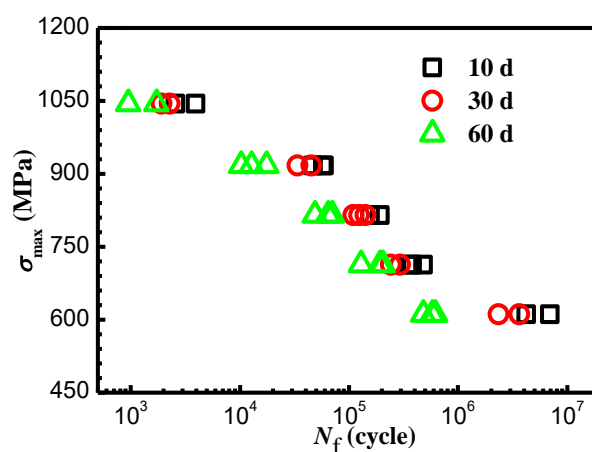


Figure 11. Fatigue test results of S135 steel after pre-corrosion in 3.5 wt.% NaCl solution for different times (10 days, 30 days and 60 days).

3.3.2 Fatigue fracture mechanisms

The fatigue fracture morphologies of S135 steel after pre-corrosion in 3.5 wt.% NaCl solution for 10, 30 and 60 days are displayed in Fig. 12. It can be seen that the area of the instantaneous fracture zone become smaller with the decreasing of loading stress after pre-corrosion for 10 days (Figs. 12 (a)–(c)), and the instantaneous fracture zone accounts for about 50% and 30% of the fracture surface when the stress is 1044.5 MPa and 611.4 MPa, respectively. After pre-corrosion for 30 days, all the fatigue cracks originate at or near the corrosion pits on the surface of the specimens. As the loading stress decreasing, the area of the instantaneous fracture zone decreases. Compared with Figs. 12 (d) and (e), it is obvious that the area of the instantaneous fracture zone decreases to about 30% of the cross-section

when the stress is 611.4 MPa (Figs. 12 (f)). After pre-corrosion for 60 days, the fatigue crack initiates from the corrosion pit, and the area of the instantaneous fracture zone becomes smaller with the decreasing of the loading stress (Figs. 12 (g)– (i)).

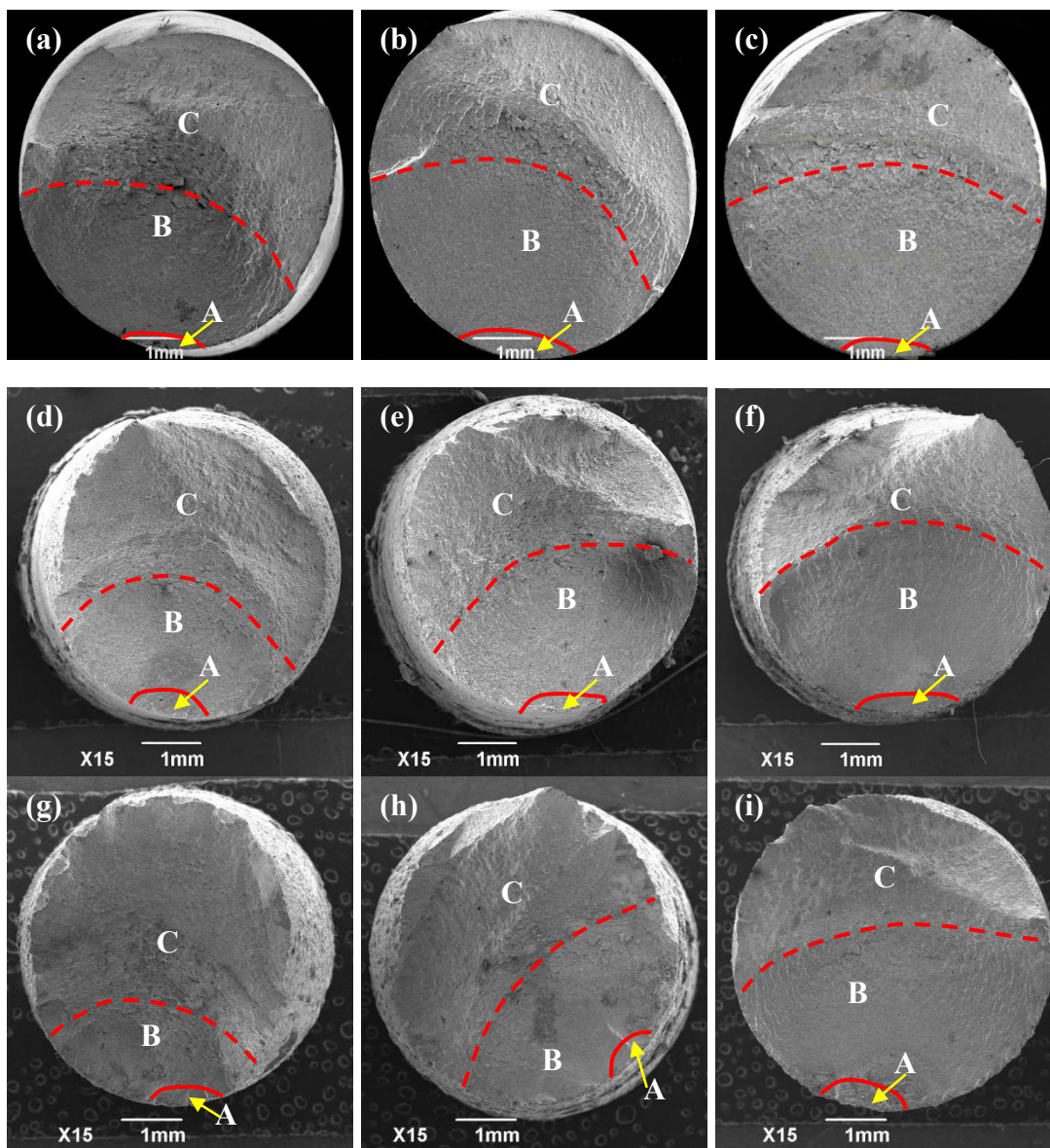


Figure 12. Fatigue fracture morphologies of S135 steel under different stress amplitudes after pre-corrosion in 3.5 wt.% NaCl solution for different times: (a) $\sigma_{\max} = 1044.5$ MPa, (b) $\sigma_{\max} = 815.2$ MPa and (c) $\sigma_{\max} = 611.4$ MPa after pre-corrosion for 10 days; (d) $\sigma_{\max} = 917.1$ MPa, (e) $\sigma_{\max} = 815.2$ MPa and (f) $\sigma_{\max} = 611.4$ MPa after pre-corrosion for 30 days; (g) $\sigma_{\max} = 1044.5$ MPa, (h) $\sigma_{\max} = 815.2$ MPa and (i) $\sigma_{\max} = 611.4$ MPa after pre-corrosion for 60 days. ‘A’ represents fatigue source zone, ‘B’ represents fatigue crack propagation zone and ‘C’ represents fracture transient zone.

Figure 13 shows the fatigue fracture micro-morphologies of the crack initiation zone on S135 steel under different stress after pre-corrosion for 10, 30 and 60 days in 3.5 wt.% NaCl solution. It can be seen that fatigue cracks initiate from the surface of the specimen after immersion for 10 days, and

obvious corrosion pits can be observed on the fracture surface (Figs. 13 (a)– (c)). The crack initiation zone is characterized by cleavage fracture, and the cleavage characteristics become more obvious with the increasing of stress amplitudes. Under the action of stress, the stress concentration on the surface of S135 steel due to the existence of corrosion pits which promotes the crack initiation, shortens the crack initiation period and accelerates the fracture failure process. The fracture morphologies of the crack source zone on S135 steel under different stress amplitudes after pre-corrosion for 30 days in 3.5 wt.% NaCl are shown in Figs. 13 (d)– (f). The fatigue crack sprouts on or near the surface of the corrosion pit. As the corrosion proceeding, more and more corrosion pits become denser and connect together to form a micro-crack, which aggravates the local stress concentration, promotes the crack initiation. The fatigue cracks originate from the corrosion pits, and multiple crack sources can be observed after pre-corrosion for 60 days in 3.5 wt.% NaCl solution (Figs. 13 (g)– (i)).

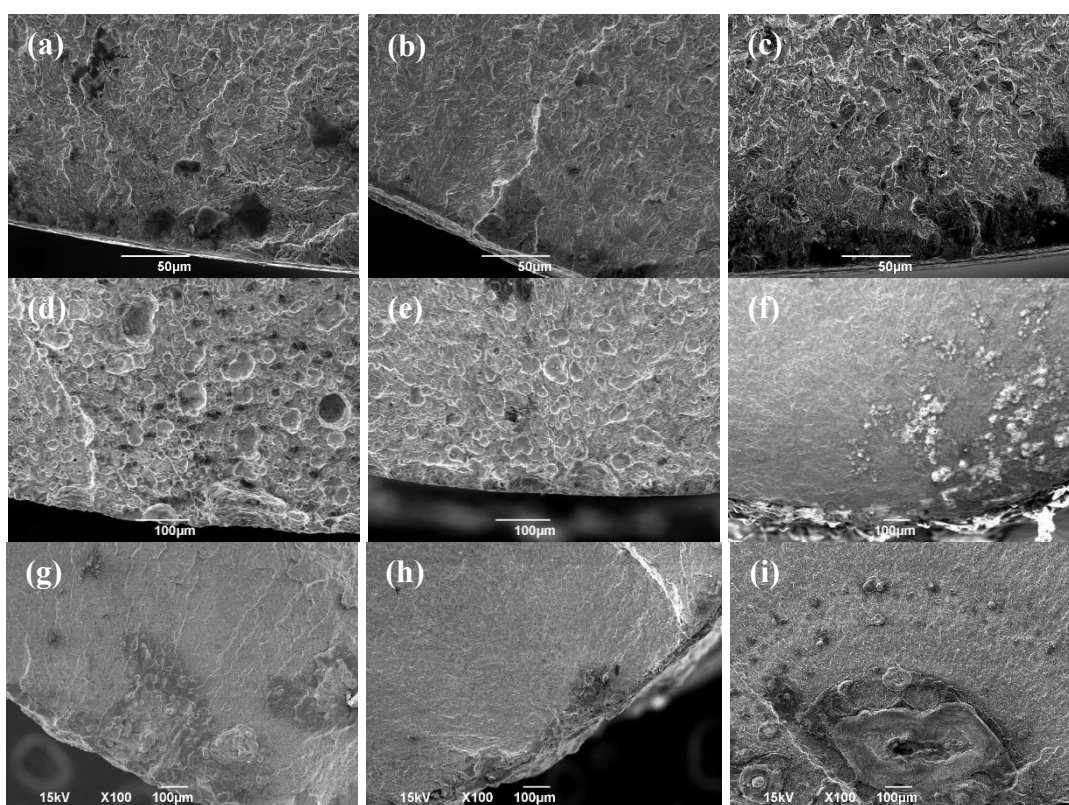


Figure 13. Fatigue fracture morphologies of crack source zone under different stress amplitudes after pre-corrosion in 3.5 wt.% NaCl solution for different times: (a) $\sigma_{\max} = 1044.5$ MPa, (b) $\sigma_{\max} = 815.2$ MPa and (c) $\sigma_{\max} = 611.4$ MPa after pre-corrosion for 10 days; (d) $\sigma_{\max} = 917.1$ MPa, (e) $\sigma_{\max} = 815.2$ MPa and (f) $\sigma_{\max} = 611.4$ MPa after pre-corrosion for 30 days; (g) $\sigma_{\max} = 1044.5$ MPa, (h) $\sigma_{\max} = 815.2$ MPa and (i) $\sigma_{\max} = 611.4$ MPa after pre-corrosion for 60 days.

Figure 14 shows the fatigue fracture morphologies of the crack propagation zone of S135 steel under different stresses after pre-corrosion for 10, 30 and 60 days in 3.5 wt.% NaCl solution. The fatigue striations and a small number of secondary cracks can be observed on the specimen after pre-corrosion for 10 days, and the fatigue striations become more obvious with the decreasing of stress amplitudes. The crack propagation zone is mainly characterized of the transgranular cleavage fracture when the stress

amplitude is 1044.5 MPa (Fig. 14 (a)); the fatigue striations become more obvious when the stress amplitude is 611.4 MPa (Fig. 14 (c)). The denser density of the fatigue striations indicate that the fatigue resistance of the material is better and the crack propagation rate is lower. Cleavage fracture is the main feature for the fatigue crack propagation zone on the specimen after pre-corrosion for 30 days, and tearing edges appear with the decreasing of stress amplitudes. The fracture is mainly characterized of cleavage fracture when the stress value amplitude is 917.1MPa (Fig. 14 (d)). A small number of fatigue striations and obvious tearing edges can be observed when the stress amplitude is 611.4 MPa (Fig. 14 (f)). Cleavage fracture and fatigue striation are the main features for the fatigue crack propagation zone on the specimen after pre-corrosion for 60 days. With the decreasing of stress amplitudes, fatigue striations become more obvious. The fracture is mainly transgranular when the stress amplitude is 1044.5 MPa (Fig. 14 (h)). A small amount of fatigue striations can be observed on the fracture surface when the stress amplitude is 611.4 MPa (Fig. 14 (i)).

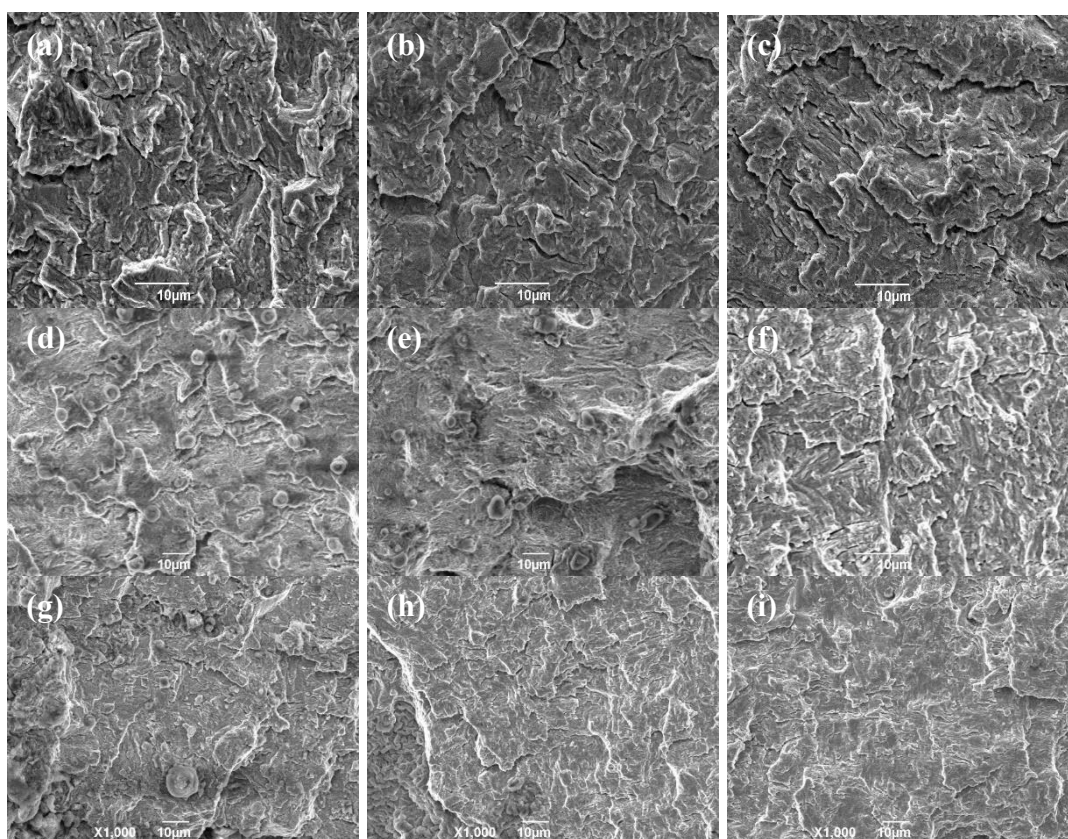


Figure 14. Fatigue fracture morphologies of crack propagation zone under different stress amplitudes after pre-corrosion in 3.5 wt.% NaCl solution for different times: (a) σ_{\max} =1044.5 MPa, (b) σ_{\max} =815.2 MPa and (c) σ_{\max} =611.4 MPa after pre-corrosion for 10 days; (d) σ_{\max} =917.1 MPa, (e) σ_{\max} =815.2 MPa and (f) σ_{\max} =611.4 MPa after pre-corrosion for 30 days; (g) σ_{\max} =1044.5 MPa, (h) σ_{\max} =815.2 MPa and (i) σ_{\max} =611.4 MPa after pre-corrosion for 60 days.

3.3.3. Fatigue mechanisms

Corrosion is the most well-known form of steel deterioration resulting in generation of pits. Fatigue cracks often start from the stress concentration area, localized corrosion in the form of pits may

provide the required conditions for initiation of fatigue crack [34,35]. Micro-cracks will germinate from the corrosion pit surface and propagate along grain boundaries when the corrosion pit grows to a certain extent, and then the transgranular crack growth will occur when the micro-crack reaches a critical length [36,37]. The SEM microstructures of the specimen section after pre-corrosion for 30 days and the corresponding schematic diagram of the transition from pitting corrosion to fatigue cracks are shown in Fig. 15, which demonstrates that cracks initiate and propagate from the bottom of the corrosion pit. It is well known that corrosion and stress exist simultaneously in the actual drilling process. Fatigue is generally considered as a leading role for the initial stage of crack initiation and propagation under the low alternating stress. When the stress amplitude is higher than σ_{sc} , fatigue and corrosion stress may act simultaneously resulting in the rapid propagation of the cracks, in fact, the characteristic of the two combined actions is a common phenomenon in the fracture behavior of the drill pipe [9]. As for the high-strength drill pipe steel, the cracks initiated from the corrosion pit are distributed parallel to different or the same horizontal planes of the pipe wall. The alternating stress increases with the decreasing of the cross section of the pipe wall, and the crack tip will propagate to the metal along the direction of wall thickness. When a crack extends to a certain length and meets with another crack, those two cracks will merge and propagate faster, and two cracks in different planes can also be connected by tearing, jumping from one plane to another [38,39]. As the crack continues to expand, the remaining wall thickness becomes thinner and thinner, and then a penetrating crack is formed. The high pressure drilling fluid penetrates through the gap and then forms a penetrating hole. When the remaining interface is insufficient to withstand the working stress, the fracture will occur.

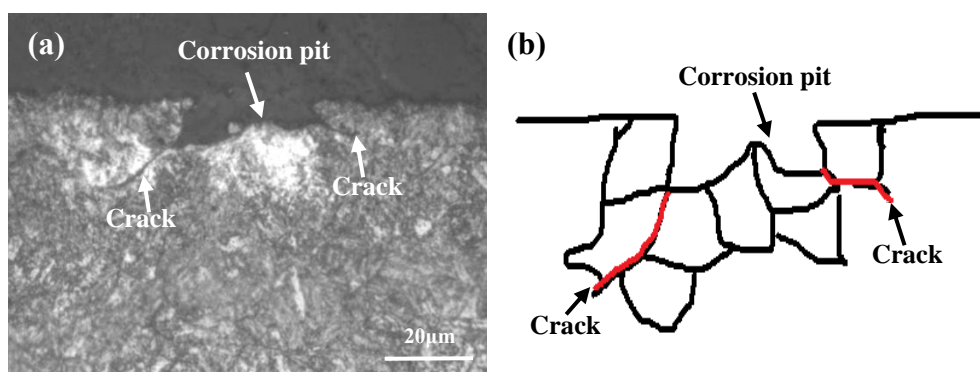


Figure 15. Scheme of transition from corrosion pit to fatigue crack of S135 steel after pre-corrosion in 3.5 wt.% NaCl solution for 30 days: (a) the corrosion pit section SEM microstructure of sample after pre-corrosion, (b) schematic diagram of the transition from pitting corrosion to fatigue cracks.

4. CONCLUSIONS

(1) With the increasing of the immersion time, OCP of S135 drill pipe steel shifts negatively, the electrochemical activity increases, and the corrosion thermodynamic stability decreases; the EIS shows two time constants; the polarization curve shows active corrosion without passivation, and the corrosion resistance decreases.

(2) The corrosion rate of S135 steel increases with the increasing immersion time; the corrosion products are mainly Fe_2O_3 , $\text{FeO}(\text{OH})$ and Fe_3O_4 , which are porous and not adhering tightly to the substrate. The size of the corrosion pits becomes larger and deeper as the corrosion time prolongs.

(3) The fatigue life of S135 steel decreases with the prolongation of pre-corrosion time. The fatigue cracks originate from the corrosion pits and multiple crack sources could be observed when the pre-corrosion time is increased. Cleavage steps and fatigue striations are the main features in the crack propagation zone, the fatigue striations become more obvious and the spacing of striations becomes smaller with the decreasing of stress amplitudes.

ACKNOWLEDGMENTS

This work was supported by the the National Natural Science Foundation of China (No. 51801149), the China Postdoctoral Science Foundation (No. 2017M620448), the Opening Project of Material Corrosion and Protection Key Laboratory of Sichuan Province (No.2018CL16), the Natural Science Foundation of Shaanxi Province of China (No. 2017JQ5031), the Scientific Research Foundation for Doctoral Program of Xi'an Shiyou University (No. 2015BS08) .

References

1. X. Tong, M. J. Dai, Z. H. Zhang, *Appl. Surf. Sci.*, 271 (2013) 373.
2. G. Yang, F. Liu, D. Pan, W. Zhang, H. Liu, C. Zeng, *Nat. Gas Ind.*, 34 (2014) 158.
3. J. J. Ryu, P. Shrotriya, *Appl. Surf. Sci.*, 273 (2013) 536.
4. T. L. Zhao, Z. Y. Liu, C. W. Du, M. H. Sun, X. G. Li, *Int. J. Fatigue*, 110 (2018) 105.
5. Y. H. Lin, J. Pan, W. Y. Liu, Q. J. Wang, Y. Pan, S. L. Wang, *Oil. Drill. Prod. Techno.*, 38 (2016) 59.
6. E. M. Mohamed, S. Nicolas, P. L. Thierry, D. Olivier, B. Olivier, *Corros. Sci.*, 133 (2018) 397.
7. T. S. Shih, Y. W. Chiu, *Appl. Surf. Sci.*, 351 (2015) 997.
8. S. M. Zamani, S. A. Hassanzadeh-Tabrizi, H. Sharifi, *Eng. Fail. Anal.*, 59 (2016) 60623.
9. P. M. Ruben, P. L. Thierry, B. Claude, P. C. Paris, *Int. J. Fatigue*, 74 (2015) 156.
10. E. I. Kryzhaniv's'Kyi, I. M. Hoisan, O. Z. Student, *Mater. Sci.*, 50 (2014) 92.
11. P. Zhang, Q. Zhu, G. Chen, H. Y. Qin, C. J. Wang, *Materials*, 8 (2015) 6179.
12. A. Yadollahi, N. Shamsaei, S. M. Thompson, A. Elwany, L. Bian, *Int. J. Fatigue*, 94 (2017) 218.
13. J. F. Adams, J. E. Allison, J. W. Jones, *Int. J. Fatigue*, 93 (2016) 372.
14. D. Z. Zeng, H. Li, G. Tian, F. Liu, B. Li, S. J. Yu, Z. Y. Ouyang, T. H. Shi, *Mat. Sci. Eng. A*, 724 (2018) 385.
15. M. N. Iلمان, *Int. J. Fatigue*, 5 (2013) 1.
16. M. Al-yasiri, M. Al-khateeb, D. S. Wen, *Corros. Eng. Sci. Techn.*, 53 (2018) 183.
17. A. Moslemizadeh, S. R. Shadizadeh, *Petrol.*, 3 (2017) 355.
18. S. J. Luo, K. Zhao, R. Wang, *J. Mater. Eng.*, 41 (2013) 40.
19. R. Wang, S. J. Luo, M. Liu, Y. Xue, *Corros. Sci.*, 85 (2014) 270.
20. M. Liu, X. Q. Cheng, X. G. Li, Y. Pan, J. Li, *Appl. Surf. Sci.*, 389 (2016) 1182.
21. P. Koteaj, J. Vican, M. Ivaã;Kovã;, *Mater. Sci. Forum*, 844 (2016) 89.
22. M. Liu, X. Q. Cheng, X. G. Li, C. Zhou, H. L. Tan, *Constr. Build. Mater.*, 30 (2017) 193.
23. M. Liu, X. Q. Cheng, G. C. Zhao, X. G. Li, Y. Pan, *Surf. Interface Anal.*, 48 (2016) 981.
24. Z. Brytan, J. Niagaj, Ł. Reiman, *Appl. Surf. Sci.*, 388 (2016) 160.
25. M. Liu, X. Q. Cheng, X. G. Li, T. J. Lu, *J. Electroanal. Chem.*, 803 (2017) 40.
26. Nace Standard RP0775-2005 Item No, 21017, [S].
27. Y. T. Ma, Y. Li, F. H. Wang, *Corros. Sci.*, 52 (2010) 1796.

28. Y. Li, Y. F. Cheng, *Appl. Surf. Sci.*, 366 (2016) 95.
29. Y. T. Ma, Y. Li, F. H. Wang, *Corros. Sci.*, 51 (2009) 997.
30. C. Y. Hu, S. W. Kou, J. J. Guo, *Adv. Mater. Res.*, 936 (2014) 1091.
31. X. G. Huang, J. Q. Xu, *J. Zhejiang Univ–Sci. A (Appl. Phys. Eng.)*, 14 (2013) 292.
32. E. N. Codaro, R. Z. Nakazato, A. L. Horovistiz, L. M. F. Ribeiro, R. B. Ribeiro, L.R.OHein, *Mat. Sci. Eng. A*, 334 (2002) 298.
33. X. G. Hung, J. Q. Xu, *Fatigue Fract. Eng. M*, 35 (2012) 606.
34. E. Arzaghi, R. Abbassi, V. Garaniya, J. Binns, C. Chin, N. Khakzad, G. Reniers, *Ocean. Eng.*, 150 (2018) 391.
35. Y. Z. Shen, H. G. Li, H. J. Tao, J. Ling, T. Wang, J. Tao, *Int. J. Electrochem. Sci.*, 10 (2015) 938.
36. S. J. Luo, M. Liu, X. Z. Lin, *Mater. Corros.*, (2018) 1. [https://doi.org/ 10.1002/maco. 201810542](https://doi.org/10.1002/maco.201810542).
37. G. J. Wang, S. S. Zhu, Y. Zhu, A. T. Xu, *Int. J. Electrochem. Sci.*, 8 (2013) 5539.
38. S. H. Li, S. Ghosh, *Int. J. Fatigue*, 141 (2006) 373.
39. D. W. Spring, S. E. Leon, G. H. Paulino, *Int. J. Fatigue*, 189 (2014) 33.

© 2019 The Authors. Published by ESG (www.electrochemsci.org). This article is an open access article distributed under the terms and conditions of the Creative Commons Attribution license (<http://creativecommons.org/licenses/by/4.0/>).